Astrophys Space Sci (2016) 361:72
DOI 10.1007/s10509-016-2660-0

ORIGINAL ARTICLE

# Modeling of the lower ionospheric response and VLF signal modulation during a total solar eclipse using ionospheric chemistry and LWPC

**Suman Chakraborty[1] · Sourav Palit[1] · Suman Ray[1] · Sandip K. Chakrabarti[1,2]**

Received: 1 September 2015 / Accepted: 12 January 2016 / Published online: 22 January 2016


**Abstract** The variation in the solar Extreme Ultraviolet (EUV) radiation flux by any measure is the most dominant natural source to produce perturbations or modulations in the ionospheric chemical and plasma properties. A solar eclipse, though a very rare phenomenon, is similarly bound to produce a significant short time effect on the local ionospheric properties. The influence of the ionizing solar flux reduction during a solar eclipse on the lower ionosphere or, more precisely, the D-region, can be studied with the observation of Very Low Frequency (VLF) radio wave signal modulation. The interpretation of such an effect on VLF signals requires a knowledge of the D-region ion chemistry, which is not well studied till date. Dominant parameters which govern the ion chemistry, such as the recombination coefficients, are poorly known. The occurrence of events such as a solar eclipse provides us with an excellent opportunity to investigate the accuracy of our knowledge of the chemical condition in this part of Earth's atmosphere and the properties which control the ionospheric stability under such disturbances. In this paper, using existing knowledge of the lower ionospheric chemical and physical properties we carry out an interpretation of the effects obtained during the total solar eclipse of 22 of July 2009 on the VLF signal. Data obtained from a week long campaign conducted by the Indian Centre for Space Physics (ICSP) over the Indian subcontinent has been used for this purpose. Both positive and negative amplitude changes during the eclipse were observed along various receiver locations. In this paper, data for a propagation path between a Indian Navy VLF transmitter named VTX3 and a pair of receivers in India are used. We start from the observed solar flux during the eclipse and calculate the ionization during the whole time span over most of the influenced region in a range of height. We incorporate a D-region ion-chemistry model to find the equilibrium ion density over the region and employ the LWPC code to find the VLF signal amplitude. To tackle the uncertainty in the values of the recombination coefficients we explore a range of values in the chemical evolution model. We achieve two goals by this exercise: First, we have been able to reproduce the trends, if not the exact signal variation, of the VLF signal modulations during a solar eclipse at two different receiving stations with sufficient accuracy purely from theoretical modeling, and second our knowledge of some of the D-region ion-chemistry parameters is now improved.

**Keywords** Ionosphere · D-region · VLF · Solar eclipse response · Obscuration function · Ionospheric disturbances

## 1 Introduction

The ultraviolet component of the solar spectrum is the major driver of whole of Earth's ionospheric processes. The ionosphere is practically sustained by the ionization effect of this component. During day time, the upper atmosphere of the Earth absorbs most of the quiet solar radiation resulting in heating, ionization, and dissociation of the constituents there. Various recombination and attachment processes along with these dissociation and detachment mechanisms determine the quasi-stable concentrations of ions and molecules in different regions of the ionosphere in the day time. During night, mainly recombination processes are

✉ S. Chakraborty
suman.chakrabarty37@gmail.com

1 Indian Centre for Space Physics, 43 Chalantika, Garia Station Road, Kolkata 700084, India

2 S N Bose National Centre for Basic Sciences, JD Block, Salt lake, Kolkata 700098, India

present. The lowest part of the ionosphere exhibits a behavior altogether different from that of the upper counterparts, namely, E and F regions. At about 65–90 km, namely, the D-region, the ion densities originated during day time vanish completely due to recombinations at night. The hydrogen Lyman-alpha radiation from the quiet Sun is solely responsible in producing the D-layer at day time. Analyzing the effects of short and long term solar activities requires an adequate knowledge of the ion production or loss parameters, such as the absorption coefficient, ionization efficiency, various recombination rate coefficients, and efficiencies. Particularly for the D-region, the knowledge is most incomplete till date. On the other hand, investigation of the effects of various solar activities could be used to acquire better knowledge of the physical and chemical properties of this region. A solar eclipse, though very rare, is a natural phenomenon which can provide us with an opportunity to investigate these properties.

The influence of the gradual short duration shadowing and unshadowing of the part of the ionosphere under the eclipsed solar illumination can be examined by the observation of very low frequency (VLF) signal modulation. Many such observations have been carried out for different eclipses to date (e.g., Bracewell 1952; Sengupta et al. 1980; Lynn 1981; Buckmaster and Hansen 1986; Mendes da Costa et al. 1995). With the Indian Centre for Space Physics (ICSP) we were privileged to organize an extensive campaign to obtain VLF perturbation data during the total solar eclipse on 22 July 2009 from receivers spread across different parts of India and Nepal. We have collected data from a dozen of receivers (Gyrator 3). For the details of the VLF campaign, see Chakrabarti et al. (2010, 2011).

Throughout the literature, the interpretations of the observations of the effects of the eclipse are given in terms of the modification of the effective reflection height for VLF in the D-region ionosphere. Clilverd et al. (2001) presented results of their modeling for the total solar eclipse on August 11, 1999. In Europe with five receiving sets they had observational results for over 17 different paths with path lengths varying from 90 km to 14,510 km. These authors varied the values of Wait's parameter $\beta$ (sharpness) and $h'$ (effective reflection height) away from those under the normal (non-eclipsed) condition to reproduce the observed VLF amplitude and phase modulation during eclipse. They found a small increase in the values of those parameters for long paths and a large increase for short paths. Rocket experiments (e.g., Mechtly et al. 1972; Ulwick 1972) confirm such changes. Some other such works, by Ohya et al. (2012) and Pal et al. (2012), have been done basically along the same line. The work of Pal et al. (2012) is worth of special mention since this dealt with the empirical modeling of the effect of the solar eclipse on same observed data and transmitter–receiver pairs used in the current paper. They analyzed the signal variations along four propagation paths, namely, VTX-Kolkata, VTX-Malda, VTX-Raiganj, and VTX-Kathmandu and concluded that the appearance of positive and negative deviations of the signals during the eclipse depends on the occurrence of the constructive or destructive interference between the sky wave and the ground wave. They concluded that a positive deviation occurs for 1946 km VTX-Kolkata propagation path and negative deviation occurs for the remaining propagation paths, which are slightly longer than 2000 km.

Although empirical models mentioned above may have reproduced the observed deviations, they do not directly use physical and chemical processes occurring at the affected region of the ionosphere, such as ionization interactions and the stabilization mechanism, which are responsible for the observed deviation of the VLF signal. Clilverd et al. (2001) presented their model result based on the $\beta$ and $h'$ adjustment to reproduce observed VLF signal during solar eclipse at various stations in Europe. They also used a D-region ion-chemistry model where the ionization rate is calculated from a solar spectrum. They compared the electron densities calculated from Wait's parameters obtained from the VLF observation with those obtained from their ion-chemistry model. Pal et al. (2012) and Singh et al. (2012) have presented a similar Wait parameter-based interpretation of VLF observations during a solar eclipse. Those papers originated from the needs of using VLF remote sensing to monitor the D-region. The approach taken in this work is a bit different. We have attempted to reproduce the observed VLF signal on the 22 July 2009 solar eclipse in India with the help of an ionization rate calculation due to solar EUV during the eclipse followed by a simple D-region ion-chemistry model and Long Wave Propagation Capability (LWPC) code (Ferguson 1998) for finding the VLF modulation. Since the modeling of the VLF wave propagation is a multi-parameter one, we have to make a few assumptions; these will be stated in due course. Clearly the scope of application of the approach presented in our paper is different from the previous works.

The ionization rate is calculated following the formalism of Chapman (Rees 1989) from satellite data of solar flux at different altitude of the lower ionosphere and fed into a simple ion chemistry model, namely the Glukhov–Pasko–Inan (GPI) model (Glukhov et al. 1992), which, instead of dealing with numerous chemical rate equations, divides various ion densities into four broad species and solves four differential equations governing the rate of evolution of four types of ion species. In our chemistry model the ionospheric rate parameters are not known for certain. A comparison of the VLF signal amplitude perturbation simulated with different sets of values of these parameters with the observed perturbation gives us an opportunity to estimate the values of these parameters up to certain accuracy. So, in this paper we achieve

two new results, the first one being a reproduction of the observed modulation of the VLF signals and hence changes in the lower ionosphere during a solar eclipse by theoretical and numerical methods, and second one is the improvement of the ionospheric recombination properties through the trial models.

## 2 Observation of VLF: ICSP VLF campaign during solar eclipse

On 22 July 2009 a total solar eclipse occurred, the path of the totality of which crossed through India and its neighboring countries as shown in Fig. 1. The Indian Centre for Space Physics (ICSP) conducted a VLF campaign to collect VLF signals before, after, and during this eclipse day. We have received VLF signals from several places in India and Nepal. We concentrated on signals transmitted from VTX (frequency: 18.2 kHz, latitude: 8.43° N, longitude: 77.73° E). We have used a loop antenna and ICSP made Gyrator-III type receiver to receive VLF signals. The loop antenna is made on a 1 m × 1 m square frame which detects the fluctuation in magnetic field of the signals. The data is obtained through the sound card and is automatically logged into the computer as an ASCII file. The Gyrator-III is capable of giving the amplitude of the VLF signal only and, thus, we are not able to model any phase observations. The spectrum software is used for continuous data acquisition and data analysis purpose.

As VLF acquires the information on ionospheric conditions along its propagation path, any effects of modulation of electron (ion) densities in any part of its propagation path would have modified the received signal. In our case, though the eclipse was a total one, the whole or parts of the propagation paths were only affected partially. There should not be a drastic difference in the characteristics in the ionospheric modulation due to the total and the partial eclipse. In both cases the effect is equivalent to a virtual nighttime situation, the difference only lying in the magnitude of modulation.

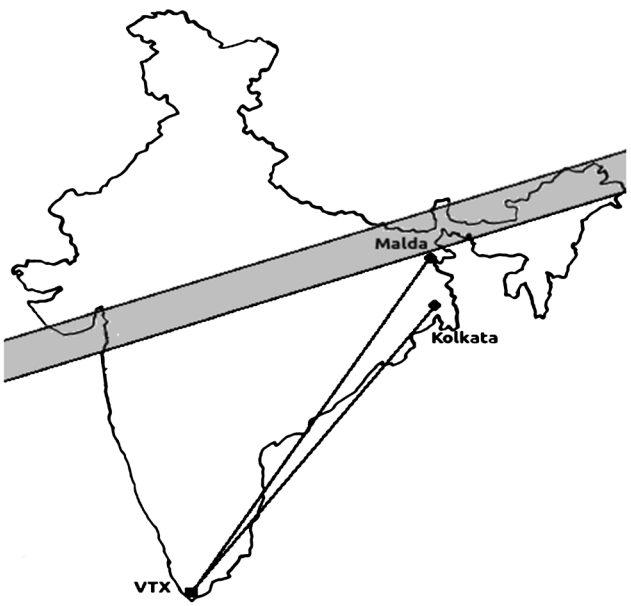


**Fig. 1** Eclipse shadow region across India, shown by the *gray belt*. The figure also shows the VTX-Kolkata and VTX-Malda paths

We have observed changes in VLF signal amplitude due to ionospheric perturbation caused by the total solar eclipse. We noticed two types of changes. In some places we found a positive change in the VLF signal amplitude, i.e., the signal amplitude increases during the solar eclipse time period, while in some other places we found a negative change in the VLF signal amplitude, i.e., the signal amplitude decreases during the eclipse (see Chakrabarti et al. 2012). In the present paper, we have compared diurnal variation of VLF signals of the eclipse day with results obtained on a non-eclipse (normal) day for two different propagation paths. By a normal day signal, we mean the average of the signal of the day before and after the eclipsed one, i.e., 21 and 23 July, 2009. One is the VTX-Kolkata (receiver located at 22.56° N, 88.36° E) propagation path, where we have found the positive change in amplitude, and the other one is the VTX-Malda (receiver located at 25° N, 88.15° E) propagation path, where we have observed negative changes in amplitude of the VLF signals due to the effect of the eclipse. We have normalized these VLF signals by using the coupled model, made by our own simulated data and LWPC code.

In Fig. 2(a) we plot the whole day variation of signal amplitude for the VTX-Kolkata propagation path for both eclipse and normal days to compare the signal amplitude of the two situations. In Fig. 2(b) we plot the same for VTX-Malda propagation path. In the whole day signal variation, we find that during nighttime, particularly for the Kolkata receiving station between 0 to 240 minutes UT and 1140 to 1440 minutes UT there are significant variations. As during those times no part of the propagation paths were sunlit these variations are surely not due to the effect of a solar eclipse. These signal variations are due partly to the fact that at nighttime the reflecting regions of the ionosphere are more variable and partly because of the presence of a greater number of Earth-ionosphere waveguide modes resulting complicated interference pattern and greater sensitiveness to ionospheric changes (Thomson et al. 2007). We are not interested in those variations and restrict ourselves to the time approximately from 330 minutes to 450 minutes UT as shown between the two dashed lines in Fig. 2, when the solar eclipse was observed from Earth. At this time for VTX-Kolkata path we obtained a positive change, while for VTX-Malda we obtained a negative change in VLF amplitude during the eclipse with respect to the normal day.

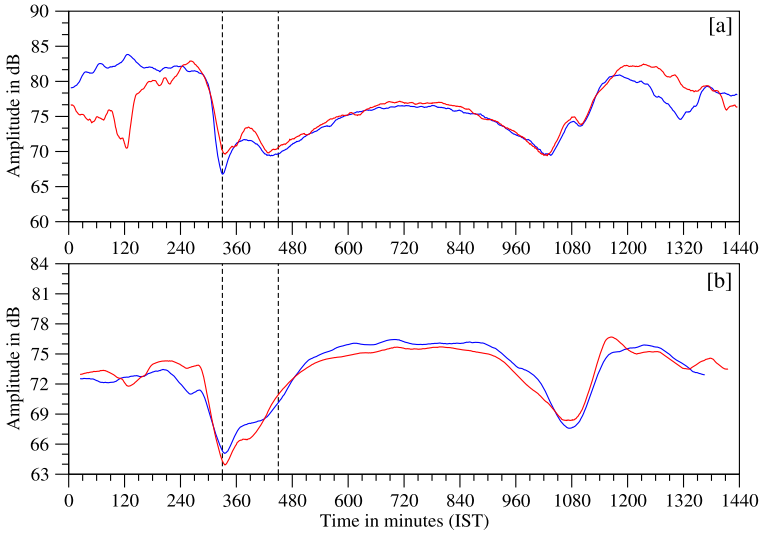


**Fig. 2** Observed diurnal amplitude of VLF signals received at Kolkata (**a**) and Malda (**b**) for both normal (*blue lines*) and eclipse (*red lines*) days. The regions enclosed by two *dashed vertical lines* in the two figures represent the part of the diurnal signal amplitude effected by the solar eclipse

## 3 Simulation of the VLF modulation during total solar eclipse

According to the mode theory (Budden 1961; Wait and Spies 1964), the very low frequency signal at certain frequency at a receiver is a superposition of the electric field associated with various modes originated from the transmitter and reaching the receiver point after being reflected and attenuated within the Earth-ionosphere waveguide. The effective layer of the ionosphere from which the wave reflects varies with the wave frequency and the electron densities of the layers. Any variation of the solar flux which could affect the electron distribution in the lower ionosphere (generally represented by Wait's formula (Wait and Spies 1964)) is determined with two parameters, namely the effective reflection height ($h'$) and the conductivity gradient or sharpness parameter ($\beta$), which in turn can modulate the VLF signal. During solar eclipse due to temporary shadowing of the ionosphere under the influence of the eclipse the electron density undergoes a temporary but gradual fall raising the effective reflection height. Depending on the propagation path and the change in interference pattern between the various modes the VLF signal amplitude can increase and decrease during the eclipse. We first calculated the ionization rates starting from approximate eclipse modulated solar spectrum during the time of the eclipse and fed them into the simple ion chemistry program (GPI model) to find the equilibrium electron density at different heights. The simulated height varying electron density values are then employed to find the VLF modulation.

### 3.1 Calculation of ionization rate

For normal solar conditions, i.e., in the absence of any activity, the height variation of the ionization rate at any instant of time can be assumed to be governed by the incident EUV spectrum only (Yonezawa 1966; Rees 1989). An ionization rate, $q$, due to EUV-ray as a function of time ($t$) and height ($h$) can be expressed after a suitable modification of Chapman's formula (Chapman 1931; Mitra 1951), given by

$$q(h,t) = \sum_j \int I_0(\nu,t) e^{-\sum_k \sigma_k(\nu) \int_h^\infty n_k C_h(h,\psi)]\,\mathrm{d}h} \times \eta_j(\nu)\sigma_j(\nu) n_j(h)\,\mathrm{d}\nu, \quad (1)$$

where $I_0(\nu,t)\,\mathrm{d}\nu$ is the irradiance or the solar flux at the top of the atmosphere in the frequency range $\nu$ to $\nu+\mathrm{d}\nu$, $\sigma_j(\nu)$ is the absorption cross section for the $j$th neutral component of air, which is a function of the energies of the photons. $n_j(h)$ is the concentration and $\eta_j(\nu)$ is the photo ionization efficiency for the $j$th component. $C_h(h,\psi)$ is the grazing incidence function and is given by Rees (1989)

$$\int_{h_0}^{\infty} n_j C_h(h,\psi)\,\mathrm{d}h = \int_{h_0}^{\infty} n_j \left[1 - \left(\frac{R_\mathrm{e}+h_0}{R_\mathrm{e}+h}\right)^2 \sin^2(\psi)\right]^{\frac{1}{2}} \mathrm{d}h,$$

for $\psi < 90°$ and

$$\int_{h_0}^{\infty} n_j C_h(h,\psi)\,\mathrm{d}h = 2\int_{h_{\min}}^{\infty} n_j \left[1 - \left(\frac{R_\mathrm{e}+h_{\min}}{R_\mathrm{e}+h}\right)^2\right]^{\frac{1}{2}} \mathrm{d}h - \int_{h_{\min}}^{\infty} n_j \left[1 - \left(\frac{R_\mathrm{e}+h_{\min}}{R_\mathrm{e}+h}\right)^2 \sin^2(\psi)\right]^{\frac{1}{2}} \mathrm{d}h, \quad (2)$$

for $\psi > 90°$.

Here $\psi$ is the solar zenith angle, $R_e$ is the mean radius of the Earth, and $h_{min}$ is the minimum height along the photon path and it is given by $h_{min} = \cos(\psi - 90°)(h_0 + R_e) - R_e$.

There are several works in the literature on the absorption cross section and photo ionization efficiencies, such as Torr et al. (1979) for $N_2$, $O_2$ and $O$, Ohshio et al. (1966) for $NO$ and $Ar$ and Mecwan and Philips (1975) for $CO_2$. The values of those coefficients and the reference spectrum of the Sun for the value of $F_{10.7} = 68$, from Torr et al. (1979), with some values of intensities collected from the well-known literature are documented in Turunen et al. (1992). We have tabulated the values we have used in our calculations in Table 1. The spectrum described in the list is taken as the reference spectrum and normalized accordingly. The normalization for different solar activity levels for intensities could be done in terms of chosen level of solar activity ($F_{10.7}$ value), but as this value is measured on a day-by-day basis and only daily average values are available, we prefer not to use these in our model, which is aimed for few minutes to hours only. Furthermore the reference spectrum such as used in our model and of others like Torr and Torr (1985), Bailey (1995) and Solomon and Qian (2005) are obtained from using observation results and combining different proxies of radiation from different parts of the Sun. Different indicators are used as proxy of such radiations, for example, NOAA MgII core to wing ratio, the composite H1 Lyman alpha and F10.7 are good proxies for chromospheric emission, transition region emission, and coronal emission, respectively (Woods and Rottman 2002). So only F10.7 or H1 Lyman alpha is not sufficient for normalization. We adopt a different method of normalization for our purpose as adopted by the literature, such as Reich (2008), which has employed a FISM model (Chamberlin et al. 2007) result of 60 second irradiance in 1 nm-wide bins from 0.5–192.5 nm and GOES-12 1-minute 0.04–0.5 nm and 0.1–0.8 nm X-ray flux with Qian 22-bin reference spectrum (Solomon and Qian 2005) in a modified version of SAMI2 model to evaluate the effect of solar flare on ionosphere. As we are dealing with a quiet solar situation we do not need the X-ray flux and instead of employing model results for irradiance (such as FISM model as used in Reich 2008) we rely on direct observation. According to Tsurutani et al. (2005), the TIMED Solar EUV Experiment (SEE) 0.1–194 nm spectral data indicates that the variations between 20–110 nm are very similar to that of the SOHO SEM EUV profile. From Milligan et al. (2012), which presents the time variation of different continuum flux and Lyman-alpha flux during a flare, we find that though the UV flux is dominated by Lyman-alpha line, the respective time variation of the UV continuum and Lyman alpha are very similar (irrespective of whether there is a flare or not), i.e., the ratio of energy emitted in different bands remain almost constant. These results motivate us to use 26–34 EUV flux (averaged over 15 sec) data, obtained from the Solar EUV Monitor on-board the SOHO satellite to normalize the reference spectrum. The daily averaged EUV fluxes in the 26–34 nm spectral band (http://www.usc.edu/dept/spacei_science/semdatafolder/long/15_sec_avg/2008/) are compared with the flux in the same spectral range of the reference spectrum presented in Table 1 and the latter is multiplied by the ratio of the mentioned fluxes at any time to obtain an approximate solar spectrum at times of interest. The flux is then modified by multiplying with the luminance (L) obtained from the obscuration function (p) (Möllmann and Vollmer 2006) due to the solar eclipse at any respective position along and near the eclipse shadow region. Solar zenithal variation is taken into account by the solar zenith angle $\psi$ in Eq. (2).

The geometry of the relative positions of the Sun and Moon during a solar eclipse (as depicted in Möllmann and Vollmer 2006) is shown in Fig. 3. Here $r$ is the radius of the Sun and $R$ that of the Moon as observed from the central line of the eclipse shadow, $\theta$ and $\phi$ are the angles subtended at the respective centers by the points where the perimeters cross each other, $D$ is the distance between the centers of the Sun and the Moon as seen from any shadow point on Earth and $d$ is the distance of the shadow region.

The degree of obscuration $p$ is given by the ratio of the Sun's projected area covered by the Moon to the Sun's total projected area on Earth. The formulae for the solar obscuration function and luminance ($L$) at any region of Earth under shadow are, respectively, given by

$$p = \frac{r^2(\theta - \cos\theta \sin\theta) + R^2(\phi - \cos\phi \sin\phi)}{\pi r^2}, \tag{3a}$$

$$\frac{L}{L_{max}} = 1 - p, \tag{3b}$$

where

$$\cos\theta = \frac{1}{2}\left(\frac{r^2 - R^2 + (R + r - d)^2}{r(R + r - d)}\right) \tag{4a}$$

and

$$\cos\phi = \frac{1}{2}\left(\frac{R^2 - r^2 + (R + r - d)^2}{R(R + r - d)}\right). \tag{4b}$$

From all points on Earth, specifically within the shadow region, the angular diameter of the Sun and the Moon are almost the same (~0.5°). So as an approximation we can safely consider $r$ and $R$ to be equal, which in turn makes $\theta$ and $\phi$ similar. Then the cosines of those angles become

$$\cos\theta = \cos\phi = \frac{1}{2}\frac{D}{r}. \tag{5}$$

Also we consider the maximum illumination of the Sun ($L_{max}$) to be 1. With these, the formulae for obscuration

**Table 1** Reference solar spectrum ($F_{10.7} = 68$), absorption cross sections, and photo ionization efficiencies

| Wave length nm | Inten sity $10^9$ cm$^{-2}$ s$^{-1}$ | Absorption cross section (cm$^2$) | | | | | | Ionization efficiency | | | | | |
|---|---|---|---|---|---|---|---|---|---|---|---|---|---|
| | | $N_2$ $10^{-19}$ | $O_2$ $10^{-19}$ | $O$ $10^{-19}$ | $Ar$ $10^{-19}$ | $He$ $10^{-19}$ | $NO$ $10^{-19}$ | $N_2$ | $O_2$ | $O$ | $Ar$ | $He$ | $NO$ |
| 5–10 | 0.07668 | 6.0 | 11.8 | 10.6 | 0.0 | 2.1 | 0.0 | 1.0 | 1.0 | 1.0 | 6.16 | 1.0 | 0.0 |
| 10–15 | 0.02692 | 23.2 | 36.1 | 35.3 | 0.0 | 5.3 | 0.0 | 1.0 | 1.0 | 1.0 | 3.5 | 1.00 | 0.0 |
| 15–20 | 0.36836 | 54.0 | 72.7 | 59.6 | 0.0 | 10.2 | 0.0 | 1.0 | 1.0 | 1.0 | 2.54 | 1.0 | 0.0 |
| 20–25 | 0.1847 | 81.5 | 105 | 75.5 | 0.0 | 17.1 | 0.0 | 1.0 | 1.0 | 1.0 | 0.22 | 1.0 | 0.0 |
| 25–30 | 0.24272 | 101 | 136 | 87.8 | 0.0 | 22.8 | 0.0 | 1.0 | 1.0 | 1.0 | 0.0 | 1.0 | 0.0 |
| 30–35 | 1.4202 | 146 | 172 | 100$E$ | 0.0 | 36.5 | 0.0 | 1.0 | 1.0 | 1.0 | 0.0 | 1.0 | 0.0 |
| 35–40 | 0.1903 | 175 | 182 | 107 | 0.0 | 42.5 | 0.0 | 1.0 | 1.0 | 1.0 | 0.0 | 1.0 | 0.0 |
| 40–45 | 0.07852 | 211 | 194 | 112 | 0.0 | 55.1 | 0.0 | 1.0 | 1.0 | 1.0 | 0.0 | 1.0 | 0.0 |
| 45–50 | 0.09726 | 218 | 216 | 116 | 247 | 70.9 | 0.0 | 1.0 | 1.0 | 1.0 | 0.44 | 1.0 | 0.0 |
| 50–55 | 0.10116 | 245 | 241 | 119 | 368 | 7.2 | 0.0 | 1.0 | 1.0 | 1.0 | 0.55 | 1.0 | 0.0 |
| 55–60 | 0.5727 | 224 | 250 | 119 | 382 | 0.0 | 0.0 | 1.0 | 1.0 | 1.0 | 0.67 | 0.0 | 0.37 |
| 60–65 | 0.42492 | 232 | 260 | 122 | 393 | 0.0 | 225 | 1.0 | 1.0 | 1.0 | 0.79 | 0.0 | 0.96 |
| 65–70 | 0.04466 | 298 | 263 | 100 | 375 | 0.0 | 207 | 0.84 | 0.84 | 1.00 | 0.81 | 0.0 | 0.94 |
| 70–75 | 0.11164 | 309 | 291 | 80 | 351 | 0.0 | 206 | 0.75 | 0.82 | 1.0 | 0.85 | 0.0 | 0.78 |
| 75–80 | 0.17456 | 307 | 271 | 42.3 | 310 | 0.0 | 189 | 0.25 | 0.35 | 1.0 | 0.70 | 0.0 | 0.58 |
| 80–85 | 0.38622 | 150 | 209 | 43.8 | 0.0 | 0.0 | 177 | 0.0 | 0.29 | 1.0 | 0.0 | 0.0 | 0.54 |
| 85–90 | 0.8865 | 466 | 98.5 | 41.8 | 0.0 | 0.0 | 271 | 0.0 | 0.48 | 1.0 | 0.0 | 0.0 | 0.47 |
| 90–95 | 0.8434 | 170 | 155 | 21.2 | 0.0 | 0.0 | 338 | 0.0 | 0.6 | 1.0 | 0.0 | 0.0 | 0.45 |
| 95–100 | 1.5484 | 362 | 165 | 0.0 | 0.0 | 0.0 | 199 | 0.7 | 0.73 | 0.0 | 0.0 | 0.0 | 0.55 |
| 100–105 | 1.3648 | 0.0 | 11 | 0.0 | 0.0 | 0.0 | 179 | 0.0 | 0.25 | 0.0 | 0.0 | 0.0 | 0.6 |
| 105–110 | 0.5600 | 0.0 | 9.5 | 0.0 | 0.0 | 0.0 | 88.9 | 0.0 | 0.0 | 0.0 | 0.0 | 0.0 | 0.79 |
| 110–115 | 0.182 | 0.0 | 0.0 | 0.0 | 0.0 | 0.0 | 37.0 | 0.0 | 0.0 | 0.0 | 0.0 | 0.0 | 0.82 |
| 115–120 | 0.88 | 0.0 | 0.0 | 0.0 | 0.0 | 0.0 | 27.1 | 0.0 | 0.0 | 0.0 | 0.0 | 0.0 | 0.86 |
| 120–125 | 1.6 | 0.0 | 3.06 | 0.0 | 0.0 | 0.0 | 22.1 | 0.0 | 0.0 | 0.0 | 0.0 | 0.0 | 0.76 |
| 125–130 | 0.82 | 0.0 | 0.0 | 0.0 | 0.0 | 0.0 | 22.7 | 0.0 | 0.0 | 0.0 | 0.0 | 0.0 | 0.52 |
| 130–135 | 2.48 | 0.0 | 29.0 | 0.0 | 0.0 | 0.0 | 25.2 | 0.0 | 0.0 | 0.0 | 0.0 | 0.0 | 0.23 |
| 25.63 | 0.2713 | 96.5 | 128 | 84.3 | 0.0 | 21.6 | 0.0 | 1.0 | 1.0 | 1.0 | 0.0 | 1.0 | 0.0 |
| 28.415 | 0.1 | 106 | 148 | 92.6 | 0.0 | 26.7 | 0.0 | 1.0 | 1.0 | 1.0 | 0.0 | 1.0 | 0.0 |
| 30.331 | 0.235 | 116 | 160 | 97.0 | 0.0 | 30.5 | 0.0 | 1.0 | 1.0 | 1.0 | 0.0 | 1.0 | 0.0 |
| 30.378 | 6 | 116 | 160 | 97.2 | 0.0 | 30.5 | 0.0 | 1.0 | 1.0 | 1.0 | 0.0 | 1.0 | 0.0 |
| 30.807 | 0.7394 | 180 | 184 | 10.8 | 0.0 | 43.5 | 0.0 | 1.0 | 1.0 | 1.0 | 0.0 | 1.0 | 0.0 |
| 46.522 | 0.18 | 268 | 204 | 113 | 299 | 65.3 | 0.0 | 1.0 | 1.0 | 1.0 | 0.55 | 1.0 | 0.0 |
| 55.437 | 0.7992 | 247 | 256 | 121 | 381 | 0.0 | 0.0 | 1.0 | 1.0 | 1.0 | 0.57 | 0.0 | 0.0 |
| 58.433 | 1.58 | 232 | 220 | 122 | 432 | 0.0 | 231 | 1.0 | 1.0 | 1.0 | 0.71 | 0.0 | 0.93 |
| 60.976 | 0.45 | 231 | 261 | 122 | 409 | 0.0 | 237 | 1.0 | 1.0 | 1.0 | 0.78 | 0.0 | 0.96 |
| 62.973 | 1.5 | 232 | 258 | 122 | 426 | 0.0 | 237 | 1.0 | 1.0 | 1.0 | 0.81 | 0.0 | 0.96 |
| 70.336 | 0.3915 | 263 | 250 | 113 | 363 | 0.0 | 222 | 0.88 | 0.92 | 1.0 | 0.88 | 0.0 | 0.82 |
| 76.515 | 0.1997 | 355 | 220 | 41.8 | 334 | 0.0 | 160 | 0.67 | 0.39 | 1.0 | 0.78 | 0.0 | 0.57 |
| 77.041 | 0.2425 | 269 | 252 | 41.8 | 341 | 0.0 | 160 | 0.68 | 0.39 | 1.0 | 0.78 | 0.0 | 0.57 |
| 78.936 | 0.7931 | 193 | 267 | 42.8 | 0.0 | 0.0 | 171 | 0.53 | 0.41 | 1.0 | 0.0 | 0.0 | 0.56 |
| 97.702 | 5.957 | 7.0 | 40.0 | 0.0 | 0.0 | 0.0 | 196 | 0.0 | 0.63 | 0.0 | 0.0 | 0.0 | 0.54 |
| 102.572 | 4.375 | 0.0 | 16.0 | 0.0 | 0.0 | 0.0 | 194 | 0.0 | 0.63 | 0.0 | 0.0 | 0.0 | 0.52 |
| 103.191 | 3.184 | 0.0 | 11.2 | 0.0 | 0.0 | 0.0 | 138 | 0.0 | 0.0 | 0.0 | 0.0 | 0.0 | 0.62 |
| 103.761 | 1.63 | 0.0 | 10.8 | 0.0 | 0.0 | 0.0 | 130 | 0.0 | 0.0 | 0.0 | 0.0 | 0.0 | 0.65 |
| 110.8 | 0.24 | 0.0 | 0.005 | 0.0 | 0.0 | 0.0 | 44.3 | 0.0 | 0.63 | 0.0 | 0.0 | 0.0 | 0.82 |
| 121.56 | 232 | 0.0006 | 0.10 | 0.0 | 0.0 | 0.0 | 24.0 | 0.0 | 0.0 | 0.0 | 0.0 | 0.0 | 0.81 |

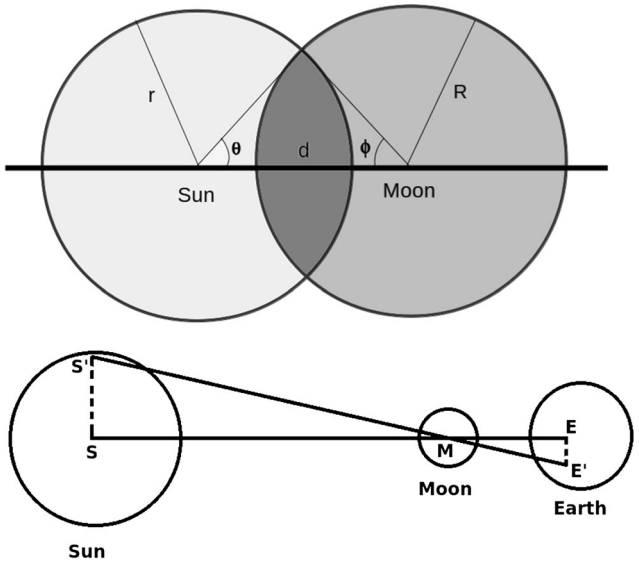


**Fig. 3** Geometry of relative positions of the solar and lunar discs during a solar eclipse (Möllmann and Vollmer 2006)

function and illuminance are modified to

$$p = \left(\frac{2}{\pi}\right)(\theta - \cos\theta \sin\theta), \tag{6a}$$

$$L = 1 - p. \tag{6b}$$

We find that the degree of obscuration at any point within the shadow is determined by the respective angular distance of the centres of the Sun and the Moon as observed from this point. We can find the quantity $D$, i.e., the angular separation between the centers of the Sun and the Moon following Fig. 3. From the picture at the lower panel of Fig. 3 we find that the center of the Sun, the Moon, and a point at the central line of the eclipse on Earth fall on the straight line SME. For any other point E′ inside the eclipse shadow on Earth the corresponding separation between the centers of Sun and Moon is given by

$$D = \frac{\mathrm{SS'}}{\mathrm{SM}} = \frac{\mathrm{EE'}}{\mathrm{ME}}. \tag{7}$$

Substituting the value of $D$ from Eq. (7) in Eq. (5), we get the value of $\cos\theta$ and then from Eqs. (6a) and (6b) we get $p$ and the corresponding $L$.

Using these formulae we calculate the degree of obscuration as a function of time for different locations. Next, to find the variation of solar EUV flux during the solar eclipse, we multiplied the obtained obscuration function with the EUV flux obtained from the Solar Extreme Ultraviolet Monitor (SEM). Combining this information with solar zenith angle variations we calculate numerically the ionization rate as a function of time and altitude. The altitude variation of ionization rate $q(h, t)$ obtained from Eq. (1) is fed into the ion chemistry model of the D-region as described below.

### 3.2 Ion chemistry model for equilibrium ion densities

The ionosphere continuously undergoes processes related to the production and loss of various types of ion species. These processes comprise the attachment of electrons to neutral molecules to form negative ions, the photo-detachment of electrons from negative ions, and the recombination of positive molecular ion and cluster ions with electrons and ion–ion recombination processes. Rather than dealing with the evolution of many different ions and their reaction cross sections, as proposed by many workers (e.g., Rowe et al. 1974; Mitra 1981; Chamberlain and Hunten 1987), we adopt a simplified model, the GPI model (Glukhov et al. 1992) to account for the chemical processes in the ionospheric D-region, through which the ionosphere tries to get back to its normal unperturbed condition. We have found very satisfactory results with this scheme in many of our previous works (e.g., Palit et al. 2013, 2014). The GPI scheme divides all the ions in four broad categories, namely free electrons ($N$), negative ions ($N^-$), positive ions ($N^+$) and positive cluster ions ($N_x^+$). Four first order coupled differential equations, governing the rate of evolution of four broad kinds of ion species are solved in the model while taking into account the neutrality of the plasma which requires that the total number of all negative and positive charges are equal always.

The coupled differential equations have been solved with the fourth order Runge–Kutta method in our modeling and are given here:

$$\frac{\mathrm{d}N}{\mathrm{d}t} = q + \gamma N^- - \beta N - \alpha_d N N^+ - \alpha_d^c N N_x^+, \tag{8}$$

$$\frac{\mathrm{d}N^-}{\mathrm{d}t} = \beta N - \gamma N^- - \alpha_i N^- \left(N^+ + N_x^+\right), \tag{9}$$

$$\frac{\mathrm{d}N^+}{\mathrm{d}t} = q - B N^+ - \alpha_d N N^+ - \alpha_i N^- N^+, \tag{10}$$

$$\frac{\mathrm{d}N_x^+}{\mathrm{d}t} = B N^+ - \alpha_d^c N N_x^+ - \alpha_i N^- N_x^+. \tag{11}$$

The D-region charge neutrality condition reads

$$N^+ + N_x^+ = N + N^-, \tag{12}$$

or

$$N^+ + N_x^+ = (1 + \lambda) N. \tag{13}$$

Here, $\lambda$ is the ratio of negative ion density to electron density.

The electron attachment rate coefficient $\beta$ determines the rate of loss of free electrons and hence production of negative ions due to the attachment of free electrons with neutral atoms and molecules, the coefficient $\gamma$ determines the rate of detachment of electrons from negative ions. The third and fourth terms in the R.H.S. of Eq. (8) corresponds to the

loss of a free electron due to dissociative recombination with positive ions and positive cluster ions, respectively. This is a chemical process in which a positive molecular ion recombines with an electron, and, as a result, the neutral molecule dissociates. $\alpha_d$ and $\alpha_d^c$ are the dissociative recombination coefficients with positive and positive cluster ions, respectively. The effective coefficients of ion–ion recombination processes for all types of positive ions with negative ions are termed $\alpha_i$ and $B$ is the effective rate of conversion from positive ions ($N^+$) to positive cluster ions ($N_x^+$).

It can be seen that with some approximation (Palit et al. 2014) the set of four equations (Eqs. (8)–(11)) can be decoupled to a single and well-known continuity equation for the D-region ionosphere. Denoting the quantity

$$\alpha_d' = \frac{\alpha_d^c N_x^+ + \alpha_d N^+}{N_x^+ + N^+}. \tag{14}$$

Equation (8) modifies to

$$\frac{\mathrm{d}N}{\mathrm{d}t} = q + \gamma N^- - \beta N - \alpha_d' N\left(N^+ + N_x^+\right). \tag{15}$$

Then some rearrangement of Eq. (9) and Eq. (15), with the help of Eq. (13), gives the continuity equation (see Appleton 1953; Mitra and Jones 1954; Mitra 1963; Zigman et al. 2007)

$$\frac{\mathrm{d}N}{\mathrm{d}t} = \frac{q}{1+\lambda} - \alpha N^2,$$

or

$$\frac{\mathrm{d}N}{\mathrm{d}t} = q' - \alpha N^2, \tag{16}$$

where

$$q' = \frac{q}{1+\lambda} \tag{17}$$

and

$$\alpha = \alpha_d' + \lambda\alpha_i \tag{18}$$

is the effective recombination coefficient of the ionospheric D-region (see Mitra 1963). The computation of free electron density evolution, sufficient to determine VLF modulation during solar eclipse, can in principle be done by solving the simple and single continuity equation, but it requires the estimation of the value of the parameter $\alpha$ at all the heights of our interest during whole of the time span, which in turn demands the prior knowledge of the values of the number densities of the positive ions ($N^+$) and positive cluster ions. Though the approximation of very low value of the positive ion density compared to that of the positive cluster ion density (Palit et al. 2014) at lower edge (∼65 km) and the opposite at the upper edge (∼80 km) of the considered lower ionospheric region allow us to acquire approximate values $\alpha_d' = \alpha_d^c$ at lower height and $\alpha_d' = \alpha_d$ at the upper heights, the value of $\alpha_d'$ and hence $\alpha$ in the region in-between is most uncertain. So instead of solving the continuity equation we prefer to solve the four coupled equations numerically, in spite of the fact that there are some uncertainties in the values of the rate parameters also. A simplification of the equation governing the rate of change of electron density can also be found in Rodger et al. (1998), where the terms corresponding to detachment and attachment are given most importance.

In spite of many decades of study of the lower ionospheric chemical reaction rates, most of them are still surrounded with uncertainties. The prevalent difficulty being the absence of direct method of observation. The lower ionosphere (∼60–90 km) is out of the reach of the balloons, satellite could not be made to float at that height due to a large drag of air, the only possibility being the rocket borne experiment. The problem with the rocket experiment is that the observation time is very limited and long term observations during various normal and disturbed ionospheric situations are significantly lacking. The estimation of coefficients is mainly based on the observation of the electron, ion densities, and computing best approximation values of those using theory such as the continuity equation. Widely varying observation values have often been the source of confusion in the probable values of the parameters; for example Mitra (1975) reported an uncertainty of second–third order in values of the effective electron detachment rate ($\gamma$) obtained from two different observations of electron densities. Various ionospheric reports and review papers (e.g., Schunk and Nagy 1980, 2000; Rees 1989; Lilensten and Blelly 1999) presented the value of dissociative recombination rate differing as much as factor of 2. The obvious consequences are the difficulty in the compositional studies of the lower ionosphere (e.g., McNeil et al. 2001), as well as that in the attempt to understand the observed electron density profiles (see Zhang et al. 2000). Also laboratory experiments have been performed to investigate various rate coefficients at various environmental conditions. Phelps (1969) and Ferguson (1971) gave a detailed review of experimental outcome on the electron attachments and detachment coefficients with $O_2$, $N_2$, and $NO$ done up to that period. Aleksandrov and Anokhin (2009, 2011) gave the account of the most recent theory and experiment of attachment and detachment of electrons to oxygen. Rowe et al. (1993) and, recently, Sheehan (2004) reviewed the experimental results on the dissociative recombination of an electron with all the positive ions relevant to lower ionosphere at a range of temperature, with the former authors also discussing the process with cluster molecules also. Reports have also been published for laboratory measurement of ion–ion recombinations (e.g. McGowan 2011) and positive ion and cluster ion conversions (e.g. Bohme 2000;

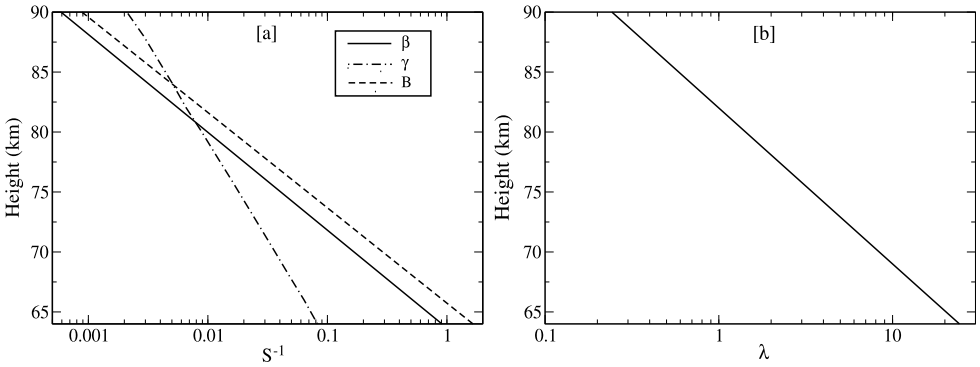


**Fig. 4** Variation of the rate coefficients with height (**a**) at the middle of the paths (corresponding to almost the same location) and that of the ratio of negative ion concentration to that of electron concentration (λ) with height (**b**)

Ryding 2011). Considering all the existing references on the rate coefficients and acknowledging that they provide a very helpful resource on the probable range of values it is best to examine or choose for the best approximation of the coefficients in those ranges to be used in any practical modeling study such as this one.

There is not much ambiguity with the value of the electron attachment rate $\beta$. It consists of two parts, one is for the three body attachment process and the other is from the two body dissociation process (Pasko et al. 1997; Haldoupis et al. 2009). The second part is only effective in the presence of a strong electric field (Lehtinen and Inan 2007) and can be neglected for the current study. The three body attachment contribution can be expressed as (Rowe et al. 1974; Glukhov et al. 1992)

$$\beta = 10^{-31} N_{O_2} N_{N_2} + 1.4 \times 10^{-29} \left(\frac{300}{T}\right) e^{(-\frac{600}{T})} N_{O_2}^2, \quad (19)$$

where $T$ is the electron temperature and $N_{O_2}$ and $N_{N_2}$ are the number densities of molecular oxygen and nitrogen, respectively. The NASA-MSIS90 atmospheric model (Hedin 1991) is used to find neutral atom concentrations at different altitudes and temperature, required for calculations of the coefficient. In Fig. 4(a) we present the altitude variation of $\beta$. As we use MSIS and IRI data for neutral molecular densities and temperature along the whole path, divided in a number of segments, the geographic (latitude and longitude) influences are automatically incorporated in the values. There have been speculative approaches (e.g., Pasko and Inan 1994; Lehtinen and Inan 2007, and references cited therein) in determining the value of effective electron detachment rate, $\gamma$. The speculated value $\gamma$ varies widely from $10^{-23} N$ s$^{-1}$ to $10^{-16} N$ s$^{-1}$ and is highly sensitive to temperature. In the line of the argument of the requirement of best choice, we first tried a standard expression of $\gamma$ taken from Pasko and Inan (1994), given by $3 \times 10^{-18} N$ s$^{-1}$. Later we varied this value in the probable range to get a better approximation of the observed results. This is discussed elaborately in the Results section.

According to certain previous studies (e.g., Chamberlain 1978; Mitra 1968; Rowe et al. 1974; Florescu-Mitchell and Mitchell 2006) the effective coefficient of dissociative recombination $\alpha_d$ should take values ranging from $10^{-7}$ to $3 \times 10^{-7}$ cm$^3$ sec$^{-1}$. Sheehan (2004) presents the variation of the quantity, obtained from various experiments, for $N_2^+$, $O_2^+$, and $NO^+$ in a wide range of temperatures. At ∼200 K, which is the typical lower ionospheric temperature, the value of the rate of dissociative recombination of the electron with an $N_2^+$ molecule is found to vary between ∼1.5–2.3 $\times 10^{-7}$ cm$^3$ sec$^{-1}$. For $O_2^+$ and $NO^+$, the corresponding ranges for the different experimental outcomes are, respectively, ∼1–3 $\times 10^{-7}$ cm$^3$ sec$^{-1}$ and ∼1–5 $\times 10^{-7}$ cm$^3$ sec$^{-1}$ from one experiment to another as described by Sheehan (2004) and references therein. We used different values of this quantity in that range to find a satisfactory matching of our results with observation. The value of the effective recombination coefficient of electrons with positive cluster ions $\alpha_d^c$ varies from $10^{-6}$ to $10^{-5}$ cm$^3$ sec$^{-1}$. In the present calculations the value has been taken to be $10^{-5}$ cm$^3$ sec$^{-1}$ as suggested by Mitra (1975) and adopted by Glukhov et al. (1992), Pasko and Inan (1994), and Haldoupis et al. (2009).

The values of effective coefficients ($\alpha_i$) of ion–ion recombination processes for all types of positive ions with negative ions is taken to be $10^{-7}$ cm$^3$ sec$^{-1}$ following Mitra (1968) and Rowe et al. (1974). The value of the effective rate of conversion ($B$) from the positive ion ($N^+$) to the positive cluster ions ($N_x^+$) is adopted to be $10^{-30} N^2$ s$^{-1}$ (Rowe et al. 1974; Mitra 1968). This is in agreement with Glukhov et al. (1992). From the simulations we have found that the influence of the variation of the last two coefficients in determining the lower ionospheric ion densities are much weaker than the others, discussed above. The values of some of the coefficients adopted in this work, those varying with height, are shown in graphs in Figs. 4(a) and (b).

Unperturbed electron and ion densities are obtained from IRI model (Rawer et al. 1978). Unperturbed negative ion density $N_0^-$ is obtained from the relationship $N_0^- = \lambda N_0$, where λ is the relative composition of the negative ions. Positive ion densities are calculated from the charge neutrality

condition, i.e.,

$$N_0 + N_0^- = N_{0x}^+ + N_0^+. \tag{20}$$

In employing this scheme it is assumed that our model time scale is so small that the physical processes, such as transport of ions through the layers, can be neglected. The outcome of the ionization rate due to EUV during solar eclipse as described above is fed into the model as $q$. Height dependent rate coefficients are calculated with the help of neutral densities obtained from MSIS 90 model data.

### 3.3 Modeling with LWPC

To reproduce the observed VLF signal variation during the eclipse time period, we have coupled our own model of electron density with the LWPC code (Ferguson 1998). The LWPC code is a collection of programs which can be used according to the user's requirement. In our case, we divided each path i.e., VTX-Kolkata and VTX-Malda into 20 segments. With the solar EUV flux modified due to the calculated obscuration function and solar zenithal variation during the eclipse, as described in the previous sections, we have calculated values of electron densities at D-region heights (64–80 km, in steps of 2 km) in each segment during the eclipse time period. The same has been calculated during the non-eclipse/normal days just before (21 July 2009) and after (23 July of 2009) the eclipse day. We then used these electron density values as the input of the LWPC code and calculated the amplitude variation of the VLF signals for both eclipse and two non-eclipse days. We used the collision frequency profile (as a function of height $h$) between electrons and neutrals as described by Kelley (2009), which is given by the following equation:

$$\nu_e(h) = 5.4 \times 10^{-10} n_n T^{1/2}. \tag{21}$$

Here $T$ is the electron temperature in K and $n_n$ is the neutral density. Using the ideal gas equation and assuming the temperatures of the electrons and the ions are the same, the above equation can be expressed as (Schmitter 2011)

$$\nu_e(h) = 3.95 \times 10^{12} T^{-\frac{1}{2}} \exp(-0.145h). \tag{22}$$

The mean values of the VLF amplitude of the two ambient days have been considered as the normal, non-eclipse situation value. Finally we compare this to obtain the deviation of the VLF amplitude of the eclipse day from the normal day.

## 4 Results

Calculation of the electron density with the exact values of the parameters proposed in the GPI model (Glukhov et al. 1992) gives somewhat different results of the modeled VLF amplitude from the observed ones. So within the range of uncertainty of the values of some of the significant parameters we have tried with their alternative values to find the desired matching of the result with the observations. In Table 2, we have documented those trial values. The table provides us with some improvements over the precision of existing knowledge of those lower ionospheric chemical rate parameters.

**Table 2** Trial parameters values in GPI chemical model and results

| $\gamma(s^{-1})$ $\times 10^{-18} N$ | $\alpha_d(\mathrm{cm^3\,s^{-1}})$ $\times 10^{-7}$ | VLF deviation at eclipse max | |
|---|---|---|---|
| | | Kolkata | Malda |
| 2.6–3 | 1 | negative | negative |
| 2.6–3 | 3 | negative | negative |
| 1–1.8 | 3 | positive | positive |
| 1.8–2.6 | 2–3 | positive | negative |

In the two stations, during the maximum eclipse, the deviation in VLF amplitude varies in sign. In Kolkata the deviation is positive, whereas in Malda it is negative during peak eclipse and the trends remain the same throughout the eclipse period. The uncertainty in the probable values of some chemical parameters allows us to vary some of their values within the anticipated range (described in Sect. 3.2) so that best agreement with the observation is achieved. As discussed in Sect. 3.2 the parameters $\alpha_d^c$, $\alpha_i$ and $B$ are less dominant in determining the chemical balance in D-region than $\beta$, $\gamma$ and $\alpha_d$. Again there exists very little ambiguity in the values of $\beta$ (given by Eq. (19)) compared to the other two parameters. Hence we have tried varying the values of the last two quantities only. In Table 2 we included the probable range of the two parameters as obtained from simulation so that we find the right trends (i.e., positive or negative deviation) of the VLF deviation at the two stations during eclipse. For best matching of our model amplitude values with the observed ones, we have used the values of $\gamma$ and $\alpha_d$ of $2.3 \times 10^{-18} N$ $\mathrm{s^{-1}}$ and 2.5 $\mathrm{cm^3\,s^{-1}}$, respectively, these values obviously reside in the ranges shown in Table 2.

The electron densities at all the heights undergo a dip during the eclipse and vary from place to place according to the obscuration experienced there. Figure 5 represents the electron density (per $\mathrm{cm^3}$) at different heights at midpoint of VTX-Kolkata (a) and VTX-Malda (b) paths, which falls in the 10th segments of each of the paths, respectively, as described in the previous subsection. A notable characteristic in the electron density profiles is the variation of the time of occurrence of the turf at different heights. In Figs. 5(a) and (b) as we go from upper heights to lower heights, the electron density minima are displaced towards the right meaning a greater delay in the occurrence of the electron density minima with respect to the maximum of the eclipse experienced

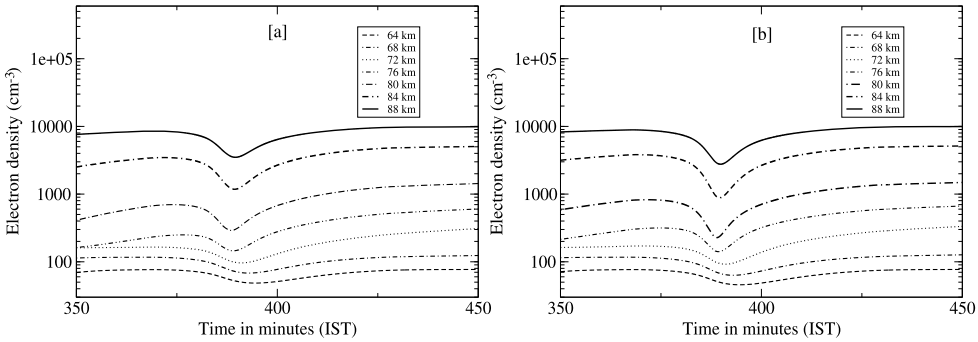


**Fig. 5** Simulated electron densities at different altitudes at middle of VTX-Kolkata (**a**) and VTX-Malda (**b**) propagation path during the solar eclipse on 22 July 2009

at that point. This is obviously the manifestation of the sluggishness in ionospheric response due to the chemical recombination processes, to the lowering of solar intensity during eclipse.

In Figs. 6(a) and (b) we show for VTX-Kolkata and VTX-Malda path, respectively, the simulated variation of VLF amplitude with distance from the transmitter for eclipse peak time (solid curve) and corresponding normal day (dashed curve) values. Each vertical dotted line represents the distance between the transmitter and receiver in the two cases. For the Kolkata path this distance is 1 946 km and for Malda it is 2 152 km.

Figures 7(a) and (b) show the VLF amplitude deviations during the eclipse from corresponding normal day values for Kolkata and Malda receiver. The solid curves represent simulated deviation and the dashed curves show observed deviation. The vertical dashed curves in both figures represent the time of the maximum obscuration at Kolkata and Malda receiving points, respectively.

The multi parametric nature of VLF propagation makes it very difficult to reproduce exact signal variation during any terrestrial or extra-terrestrial events, or even the diurnal variation. In our simulation we have been able to show starting from calculation of ionization and application of fundamental ion chemistry that at least at two different receiving points the trends of VLF signal amplitude variation during a solar eclipse match with the observed trends. We have seen in the observed data that during the peak of a total solar eclipse the signal at two different stations, separated only by ∼400 km, the change of VLF amplitude are opposite in sign, at Kolkata the VLF amplitude increases from regular values and at Malda the amplitude during eclipse maximum decreases. These are obviously manifestations of VLF mode interference. With our simulation we have been able to reproduce the trends at those two sites and also the deviations during peak time significantly match with those in the observations.

Direct verification with observation, such as rocket experiments, of our simulation results on electron density variation with height could not be done due to the scarcity of observations during solar eclipse in such a low latitude. However, a rough comparison with the electron density versus

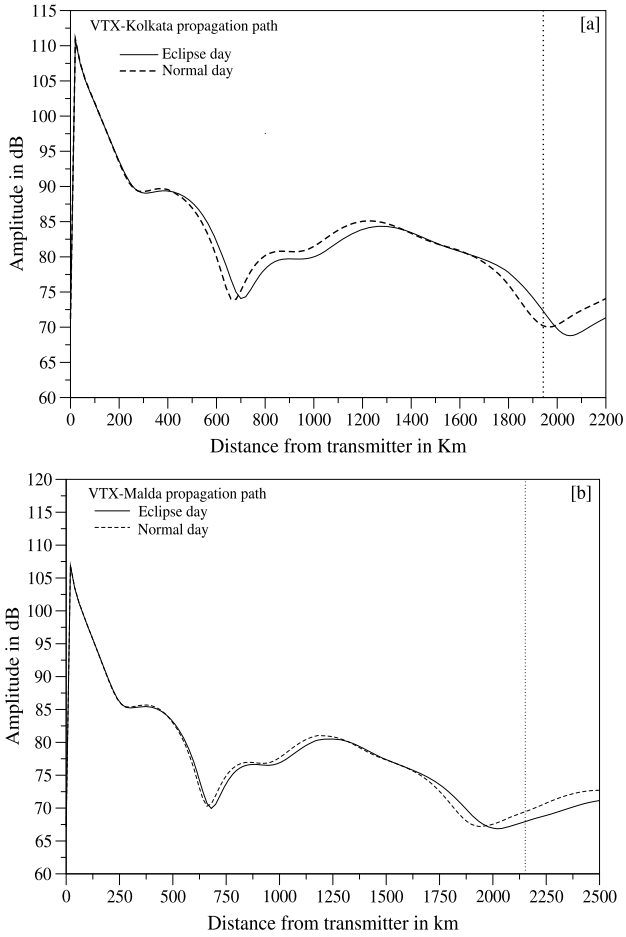


**Fig. 6** VLF amplitudes as a function of distance from the transmitter for eclipse maximum time ($t = 60$ minutes UT) for the eclipse day (*solid curve*) and normal day (*dashed curve*) for both the VTX-Kolkata (**a**) and the VTX-Malda (**b**) propagation paths. The *vertical dotted lines* in both figures represent the location of the receivers

height profile presented in Clilverd et al. (2001) shows that the simulated electron density (as presented in Fig. 5) profile in our case is somewhat higher in values and also the ratio of electron density (∼200 per cm$^3$) at lower heights (∼70 km) to that (∼80 per cm$^3$) at upper heights (∼80 km) is somewhat greater compared to that in Clilverd. It is to be noted that the electron density presented by that paper is evaluated

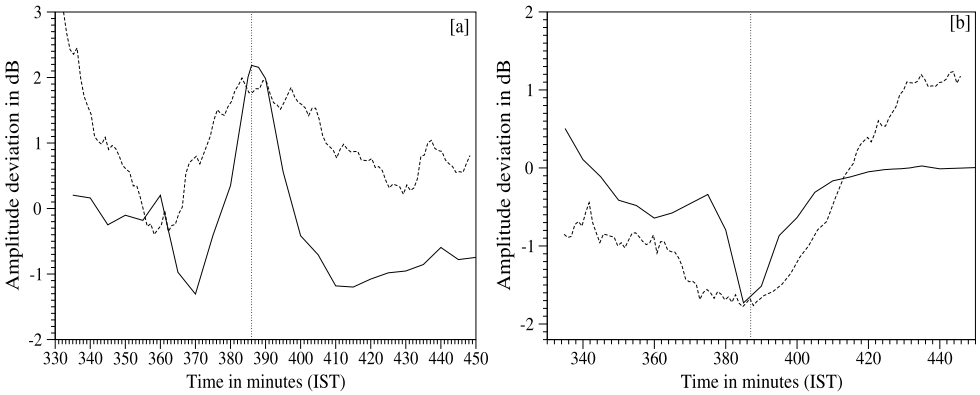


**Fig. 7** VLF amplitude deviation of eclipse-day signal from normal day signal for Kolkata (**a**) and Malda (**b**) receivers. The *solid curves* represent the simulated deviation and the *dotted curves* are those obtained from observation

**Table 3** Wait's parameter comparison

| Station | Condition | Simulation result | | Pal et al. (2012) | |
|---|---|---|---|---|---|
| | | $\beta$ | $h'$ | $\beta$ | $h'$ |
| Malda | Normal | 0.3 | 74.0 | 0.314 | 73.98 |
| Malda | Eclipse max | 0.302 | 77 | 0.318 | 76.5 |
| Kolkata | Normal | 0.35 | 76.0 | 0.34 | 75.2 |
| Kolkata | Eclipse max | 0.352 | 77.8 | 0.345 | 77.2 |

at a latitude ∼40°–50° North. It is evident that at lower latitudes, due to smaller solar inclinations, the overall electron densities at different heights should be higher than those at higher latitude in identical situations such as solar eclipses. Also due to a more direct and deeper penetration of solar UV near the equatorial regions, the relative abundance of electrons at lower heights with respect to that at higher heights should be greater than that at higher latitudes. Consequently the lower latitude places should have lower $\beta$. It may also be confirmed on comparing results of Pal et al. (2012) with Clilverd et al. (2001). We recall that the first one analyzes the influence of the same solar eclipse we are dealing with, using the same method as followed by Clilverd. From the results presented in the second one it is found that during the eclipse maximum, $\beta$ is found to be ∼0.5 and in Pal et al. (2012) it is found to be ∼0.32–0.35 at different propagation paths. Considering the scenario we can say that our result is reasonable.

Another way to compare is to find the effective values of the two Wait parameters, namely, $\beta$ and $h'$, calculated from electron densities obtained form our simulation with those presented in Pal et al. (2012), as both deals with the same solar eclipse event. It should be realized that the simulated electron density should in principle not match completely with a Wait profile of the electron density variation with height. Here we find the set of values of the two Wait parameters for which the calculated Wait profile best approximates with our result in the range of height considered here. In Table 3 we present the values for comparison.

In Fig. 8, we show the variation of electron density over Indian subcontinent at three different times and at three different heights, with respective color bars in three dimensional plots. These plots are solely obtained from the results of our chemistry model. From left to right the figures correspond to the times: 50 minutes, 1 hr, and 1 hr 10 minutes (UT) and from top to bottom they correspond to 68 km, 72 km, and 76 km altitudes, respectively. At least in two of the three heights we can see clearly the shadows of the Moon (cast in electron density profile) gradually passing from West to East as time passes during the eclipse.

## 5 Discussions and conclusions

In this paper, we have attempted for the first time to reproduce through computer simulation the modulation of VLF amplitude during solar eclipse starting from solar illumination flux. We tried to be as thorough as possible in our analysis. During solar eclipse, the ambient solar EUV is being hindered totally or partially by the Moon from place to place on Earth. We have calculated the decrease in electron density by near-exact modeling of the solar flux variation during the eclipse time with the help of data obtained from a dedicated satellite, proper estimation of the solar zenithal variation and obscuration function. In order to find variations of the VLF amplitude we have examined those electron density variations in multiple (20) places along the paths.

In only one of the cases we analyze, the VTX-Malda path, the VLF receiver is at the near-total eclipse belt for some time. So for most of the regions across the two propagation paths we considered, the obscuration of the solar disc was only partial and varying with time. Due to this and also due to the inertial properties of recombination processes, the electron density at any place does not decrease to values similar to that in nighttime. So the D-region does not cease to exist at eclipse time as seen in our simulation results of the electron density variation at different heights (Fig. 5).

There are obviously certain limitations in our modeling effort. For instance, we found the ionization by solar EUV

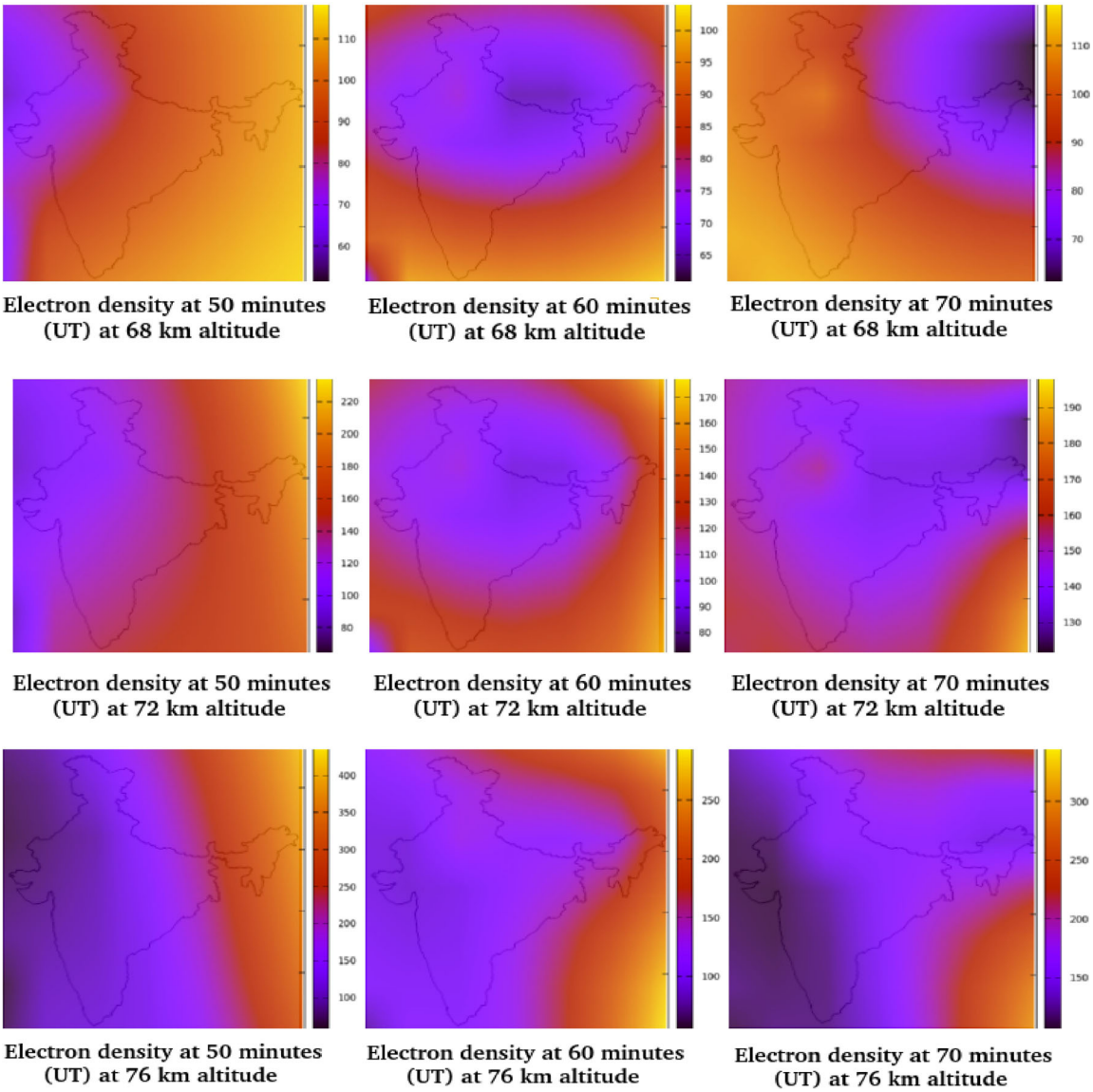


**Fig. 8** Two dimensional plots with *color bar* (values corresponding to per cubic centimeter per second) showing the shadow of the moon cast in electron density during the solar eclipse of 22 July 2009 passing through India along the course of the eclipse. The figures in the *top panel* correspond to values of electron densities at 68 km. The *middle* and *bottom panels* correspond to electron densities, respectively, at 72 km and 76 km. The *left-most figures* are of 50 minutes in UT, the *middle* and *right-most figures* correspond to 60 minutes and 70 minutes in UT, respectively

from complete theoretical calculations, with values of the coefficients acquired from the existing literature alone. The normalization schemes of the $F_{10.7} = 68$ solar flux with the SEM satellite data may not be quite accurate. The chemical model is somewhat simplified with the proposed values of the chemical coefficients by previous literature. We have employed a hitherto most efficient computation program for mode theory of VLF, namely LWPC. Though the modeled variations do not match exactly with the observations, we obtained general agreement of our results with those observed. We found that the deviation in VLF amplitude is negative for Malda and positive for Kolkata as observed. The values of maximum deviations and the time when they occur match satisfactorily. In Fig. 5, we show the variation of VLF signal amplitude with distance from the transmitter, which explains the apparently strange fact that though the two receiving points, namely Kolkata and Malda, are very close and share nearly the same obscuration along the VLF propagation paths from the transmitter to the receiver, the amplitude deviation at one point (Kolkata) is positive and at the other point (Malda) is negative during eclipse time.

Unlike previous papers (Clilverd et al. 2001; Pal et al. 2012) where conclusions have been empirically generalized based on observations at a few locations, we refrained from

such a generalization since the result must vary from point to point due to possible constructive and destructive interferences. This depends on the wavelength and therefore the transmission frequency. So sweeping statements cannot be made.

In conclusion, we must say that our model is reasonably realistic and is based on adequate physics and chemistry of the ionospheric interaction with solar radiation. Indeed, our effort appears to be successful in reproducing quite satisfactorily observations made during a solar eclipse. Thus we are somewhat closer to understanding the influences of an eclipse on the ionospheric conditions and hence on the VLF signal amplitudes. There is still some disagreement of our result with observations. This could probably be removed with a more careful study of the ionization mechanism and a determination of the ionospheric chemical model parameters.

**Acknowledgements** Suman Chakraborty and Sourav Palit acknowledge a grant from MoES for financial support. All the data are copyrighted by the Indian Centre for Space Physics, Kolkata. These may not be made public without permission of the institute.

## References

Aleksandrov, N.L., Anokhin, E.M.: Low-energy electron attachment and detachment in vibrationally excited oxygen. J. Phys. D, Appl. Phys. **42**, 225210 (2009). doi:10.1088/0022-3727/42/22/225210

Aleksandrov, N.L., Anokhin E.M.: Electron detachment from O-2 ions in oxygen: the effect of vibrational excitation and the effect of electric field. J. Phys. B, At. Mol. Opt. Phys. **44**, 115202 (2011). doi:10.1088/0953-4075/44/11/115202

Appleton, E.V.: A note on the "sluggishness" of the ionosphere. J. Geophys. Res. **3**(5), 282–284 (1953)

Bailey, S.M.: Response of the Upper Atmosphere to Variations in the Solar Soft X-ray Irradiance, Dissertation. University of Colorado, Boulder (1995)

Bracewell, R.N.: Theory of formation of an ionospheric layer below E layer based on eclipse and solar flare effects at 16 kc/sec. J. Atmos. Terr. Phys. **2**, 226–235 (1952)

Bohme, D.K.: Experimental studies of positive ion chemistry with flow-tube mass spectrometry: birth, evolution, and achievements in the 20th century. Int. J. Mass Spectrom. **200**, 97–136 (2000)

Buckmaster, H.A., Hansen, C.H.: 26 February 1979 total solar eclipse induced LF (60 kHz) phase retardation. J. Atmos. Terr. Phys. **48**, 393–397 (1986)

Budden, K.G.: The Wave-guide Mode Theory of Wave Propagation. Logos Press, London (1961)

Chakrabarti, S.K., Sasmal, S., Pal, S., Mondal, S.K.: Results of VLF Campaigns in Summer, Winter and During Solar Eclipse in Indian Subcontinent and Beyond. AIP Conf. Proc, p. 1286. AIP, New York (2010)

Chakrabarti, S.K., Pal, S., Sasmal, S., et al.: VLF Observational Results of Total Eclipse of 22nd July, 2009 by ICSP Team. IEEE Con. Publication, New York (2011)

Chakrabarti, S.K., Mondal, S.K., Sasmal, S., et al.: VLF signals in summer and winter in the Indian sub-continent using multi-station campaigns Indian. J. Phys. **86**(5), 323–334 (2012)

Chamberlain, J.W.: Theory of Planetary Atmospheres: An Introduction to Their Physics and Chemistry. Academic, San Diego (1978)

Chamberlain, J.W., Hunten, D.M.: Theory of Planetary Atmospheres: An Introduction to Their Physics and Chemistry, 2nd edn. International Geophysics Series, vol. 36, p. 481. Academic Press Inc., Florida (1987)

Chamberlin, P.C., Woods, T.N., Eparvier, F.G.: Flare irradiance spectral model (FISM): daily component algorithms and results. Space Weather **5**, 07005 (2007). doi:10.1029/2007SW000316

Chapman, S.: The absorption and dissociative or ionizing effect of monochromatic radiation of an atmosphere on a rotating Earth. Proc. Phys. Soc. **43**, 26–45 (1931)

Clilverd, M.A., Rodger, C.J., Thomson, N.R., et al.: Total solar eclipse effects on VLF signals: observations and modeling. Radio Sci. **36**(4), 773 (2001)

Ferguson: In: Laboratory Measurements of D-region Ion-molecule Reactions. Astrophysics and Space Science Library, vol. 25, pp. 188–197 (1971)

Ferguson, J.A.: Computer programs for assessment of long-wavelength radio communications. Version 2.0. Technical document 3030, Space and Naval Warfare Systems Center, San Diego (1998)

Florescu-Mitchell, A.I., Mitchell, J.B.A.: Dissociative recombination. Phys. Rep. **430**(5–6), 277–374 (2006)

Glukhov, V., Pasko, V., Inan, U.: Relaxation of transient lower ionospheric disturbances caused by lightning-whistler-induced electron precipitation. J. Geophys. Res. **97**, 16,951–16,979 (1992)

Haldoupis, C., Mika, A., Sergey, S.: Modeling the relaxation of early VLF perturbations associated with transient luminous events. J. Geophys. Res. **114**, A00E04 (2009). doi:10.1029/2009JA014313

Hedin, A.E.: Extension of the MSIS Thermosphere Model into the middle and lower atmosphere. Geophys. Res. Lett. **96**, 1159–1172 (1991)

Kelley, M.C.: The Earths Ionosphere, Plasma Physics and Electrodynamics, 2nd edn. Academic Press, San Diego (2009). Chap. 2.2

Lehtinen, N.G., Inan, U.S.: Possible persistent ionization caused by giant blue jets. Geophys. Res. Lett. **34**, L08804 (2007). doi:10.1029/2006GL029051

Lilensten, J., Blelly, P.-L.: Du Soleil à la Terre: Aéronomie et M'etéorologie de L'Espace. Presses Univ. de Grenoble, Grenoble (1999)

Lynn, K.J.W.: The total solar eclipse of 23 October 1976, observed at VLF. J. Atmos. Terr. Phys. **43**, 1309–1316 (1981)

McGowan, S.: Ion–ion recombination coefficient: II. Measurement in oxygen nitrogen mixture. Can. J. Phys. **45**(2), 439–448 (2011). doi:10.1139/p67-039

McNeil, W.J., Dressler, R.A., Murad, E.: Impact of a major meteor storm on Earth's ionosphere: a modeling study. J. Geophys. Res. **106**, 10,447–10,466 (2001)

Mechtly, E.A., Sechrist, C.F., Smith, L.G.: Electron loss coefficients for the D-region of the ionosphere from rocket measurements during the eclipses of March 1970 and November 1966. J. Atmos. Terr. Phys. **34**, 641–646 (1972)

Mecwan, M.J., Philips, L.F.: Chemistry of the Atmosphere. Edward Arnold Ltd., London (1975)

Mendes da Costa, A., Rizzo Piazza, L., Leme, P., Lower, N.M.: Ionosphere effect observed during the 30 June 1992 total solar eclipse. J. Atmos. Terr. Phys. **57**, 13–17 (1995)

Milligan, R.O., Chamberlin, P.C., Hudson, H.S., Thomas, N.W., Mathioudakis, M., Fletcher, L., Kowalski, A.F., Keenan, F.P.: Observation of enhanced EUV continua during an X-class solar flare using SDO/EVE. Astrophys. J. **748**, L14 (2012)

Mitra, A.P.: The D-layer of the ionosphere. J. Geophys. Res. **56**(3), 373–402 (1951)

Mitra, A.P., Jones, R.E.: Recombination in the lower ionosphere. J. Geophys. Res. **59**(3), 323–328 (1954)

Mitra, A.P.: Recombination in the Ionosphere Advance in Upper Atmospheric Research, pp. 57–87. Ed Landmark, London (1963)

Mitra, A.P.: A review of D-region processes in non-polar latitudes. J. Atmos. Terr. Phys. **30**(6), 1065–1114 (1968)
Mitra, A.P.: D region in disturbed condition, including flares and energetic particles. J. Atmos. Terr. Phys. **37**, 895 (1975)
Mitra, A.P.: Chemistry of middle atmospheric ionization-a review. J. Atmos. Terr. Phys. **43**(8), 737–752 (1981). ISSN 0021-9169
Möllmann, K.P., Vollmer, M.: Measurements and predictions of the illuminance during a solar eclipse. Eur. J. Phys. **27**, 1299–1314 (2006)
Ohshio, M., Maeda, R., Sakagami, H.: J. Radio Res. Lab. **13**, 245 (1966)
Ohya, H., Tsuchiya, F., Nakata, H., Shiokawa, K., Miyoshi, Y., Yamashita, K., Takahashi, Y.: Reflection height of daytime tweek atmospherics during the solar eclipse of 22 July 2009. J. Geophys. Res. (2012). doi:10.1029/2012JA018151
Pal, S., Chakrabarti, S.K., Mondal, S.K.: Modeling of sub-ionospheric VLF signal perturbations associated with total solar eclipse, 2009 Indian subcontinent. Adv. Space Res. **50**, 196–204 (2012)
Palit, S., Basak, T., Pal, S., Chakrabarti, S.K.: Modeling of very low frequency (VLF) radio wave signal profile due to solar flares using the GEANT4 Monte Carlo simulation coupled with ionospheric chemistry. Atmos. Chem. Phys. **13**, 9159–9168 (2013). doi:10.5194/acp-13-9159-2013
Palit, S., Basak, T., Pal, S., Chakrabarti, S.K.: Theoretical study of lower ionospheric response to solar flares: sluggishness of D-region and peak time delay. Astrophys. Space Sci. **355**, 2190 (2014). doi:10.1007/s1050901421906
Pasko, V.P., Inan, U.S.: Recovery signatures of lightning-associated VLF perturbations as a measure of the lower ionosphere. J. Geophys. Res. **99**(A9), 17,523–17,537 (1994)
Pasko, V.P., Inan, U.S., Bell, T.F., Tararenko, Y.N.: Sprites produced by quasi-electrostatic heating and ionization in the lower ionosphere. J. Geophys. Res. **102**, 4529–4561 (1997)
Phelps, A.V.: Laboratory studies of electron attachment and detachment processes of aeronomic interest. Can. J. Chem. **47**, 1783 (1969)
Rawer, K., Bilitza, D., Ramakrishnan, S.: Goals and status of the international reference ionosphere. Rev. Geophys. **16**, 177–181 (1978)
Rees, M.H.: Physics and Chemistry of the Upper Atmosphere. Cambridge University Press, Cambridge (1989)
Reich, P.J.: Ionospheric response to solar flares using an improved version of SAMI2. Thesis. Air force institute of technology, Ohio (2008)
Rodger, C.J., Molchanov, O.A., Thomson, N.R.: Relaxation of transient ionization in the lower ionosphere. J. Geophys. Res. Space Phys. **103**(A4), 6969–6975 (1998)
Rowe, J.N., Mitra, A.P., Ferraro, A.J., Lee, H.S.: An experimental and theoretical study of the D-region—II. A semi-empirical model for mid-latitude D-region. J. Atmos. Sol.-Terr. Phys. **36**, 755–785 (1974)
Rowe, B.R., Mitchell, J.B.A., Canosa, A.: Dissociative Recombination: Theory, Experiment, and Application. NATO ASI Series B: Physics, vol. 313, pp. 135–143. Plenum Press, New York (1993)
Ryding, M.J.: Experimental Studies of Cluster Ions Containing Water, Ammonia, Pyridine and Bisulphate: Thesis. University of Gothenburg, Sweden (2011)
Schmitter, E.D.: Remote sensing planetary waves in the midlatitude mesosphere using low frequency transmitter signals. Ann. Geophys. **29**, 1287–1293 (2011). doi:10.5194/angeo-29-1287-2011
Schunk, R.W., Nagy, A.F.: Ionospheres of the terrestrial planets. Rev. Geophys. **18**, 813–851 (1980)
Schunk, R.W., Nagy, A.F.: Ionospheres: Physics, Plasma Physics, and Chemistry. Cambridge Univ. Press, New York (2000)
Sengupta, A., Goel, G.K., Mathur, B.S.: Effect of the 16 February 1980 solar eclipse on VLF propagation. J. Atmos. Terr. Phys. **42**, 907 (1980)
Sheehan, C.H.: Dissociative recombination of $N_2^+$, $O_2^+$, and $NO^+$: rate coefficients for ground state and vibrationally excited ions. J. Geophys. Res. **109**, A03302 (2004). doi:10.1029/2003JA010132
Singh, A.K., Singh, R., Veenadharic, B., Singh, A.K.: Response of low latitude D-region ionosphere to the total solar eclipse of 22 July 2009 deduced from ELF/VLF analysis. Adv. Space Res. **50**(10), 1352–1361 (2012)
Solomon, S.C., Qian, L.: Solar extreme-ultraviolet irradiance for general circulation models. J. Geophys. Res. **110**(A10), 10,306 (2005)
Thomson, N.R., Clilverd, M.A., McRae, W.M.: Nighttime ionospheric D region parameters from VLF phase and amplitude. J. Geophys. Res. **112**(A7), A07304 (2007). doi:10.1029/2007JA012271
Torr, M.R., Torr, D.G., Ong, R.A., Hinteregger, H.E.: Geophys. Res. Lett. **6**, 771 (1979)
Torr, M.R., Torr, D.G.: Ionization frequency for solar cycle 21: revised. J. Geophys. Res. **90**, 6675 (1985)
Tsurutani, B.T., Judge, D.L., Guarnieri, F.L., Gangopadhyay, P., Jones, A.R., Nuttall, J., Zambon, G.A., Didkovsky, L., Mannucci, A.J., Iijima, B., Meier, R.R., Immel, T.J., Woods, T.N., Prasad, S., Floyd, L., Huba, J., Solomon, S.C., Straus, P., Viereck, R.: The October 28, 2003 extreme EUV solar flare and resultant extreme ionospheric effects: comparison to other Halloween events and the Bastille day event. Geophys. Res. Lett. **32**, L03S09 (2005). doi:10.1029/2004GL021475
Turunen, E., Matveinen, H., Ranta, H.: Sodankyla Ion Ccemistry(SIC) model Sodankyla Geophysical Observatory. Report No. 49. Sodankyla, Finland (1992)
Ulwick, J.C.: Eclipse rocket measurements of charged of particle concentrations. J. Atmos. Terr. Phys. **34**, 659–665 (1972)
Wait, J.R., Spies, K.P.: Characteristics of the Earth-Ionosphere waveguide for VLF radio waves. NBS Tech Note. U.S. 300 (1964)
Woods, T.N., Rottman, G.J.: Solar ultraviolet variability over the time periods of aeronomic interest. In: Atmospheres in the Solar System: Comparative Aeronomy. Geophysical Monogram, vol. 130 (2002). doi:10.1029/130GM14. AGU
Yonezawa, T.: Theory of formation of the ionosphere. Space Sci. Rev. **5**, 3–56 (1966)
Zhang, S.R., Oliver, W.L., Fukao, S., Otsuka, Y.: A study of the forenoon ionospheric F2 layer behavior over the middle and upper atmospheric radar. J. Geophys. Res. **105**, 15,823–15,833 (2000)
Zigman, V., Grubor, D., Sulic, D.: D-region electron density evaluated from VLF amplitude time delay during X-ray solar flares. J. Atmos. Terr. Phys. **69**, 775–792 (2007)